An Evaluation of UiO-66 for Gas-Based Applications

ARTICLE *in* CHEMISTRY - AN ASIAN JOURNAL · DECEMBER 2011

Impact Factor: 4.59 · DOI: 10.1002/asia.201100201 · Source: PubMed

DOI: 10.1002/asia.201100201

An Evaluation of UiO-66 for Gas-Based Applications

Andrew D. Wiersum,[a] Estelle Soubeyrand-Lenoir,[a] Qingyuan Yang,[b] Beatrice Moulin,[c] Vincent Guillerm,[d] Mouna Ben Yahia,[b] Sandrine Bourrelly,[a] Alexandre Vimont,[c] Stuart Miller,[d] Christelle Vagner,[a] Marco Daturi,[c] Guillaume Clet,[c] Christian Serre,[d] Guillaume Maurin,*[b] and Philip L. Llewellyn*[a]

Abstract: In addition to its high thermal stability, repetitive hydration/dehydration tests have revealed that the porous zirconium terephthalate UiO-66 switches reversibly between its dehydroxylated and hydroxylated versions. The structure of its dehydroxylated form has thus been elucidated by coupling molecular simulations and X-ray powder diffraction data. Infrared measurements have shown that relatively weak acid sites are available while microcalorimetry combined with Monte Carlo simulations emphasize moderate interactions between the UiO-66 surface and a wide range of guest molecules including CH_4, CO, and CO_2. These properties, in conjunction with its significant adsorption capacity, make UiO-66 of interest for its further evaluation for CO_2 recovery in industrial applications. This global approach suggests a strategy for the evaluation of metal–organic frameworks for gas-based applications.

Keywords: adsorption · calorimetry · density functional calculations · metal–organic frameworks · X-ray diffraction

Introduction

The huge amount of research devoted to metal–organic frameworks (MOFs) notably stems from the almost infinite possibility to vary their chemistry through the metal center, organic linker, as well as their geometric arrangement. The wide spectrum of materials synthesized so far could be of interest in a number of applications including gas separation and storage,[1–5] vapor adsorption,[6] liquid-phase separation,[7] energy storage,[8] and bio-applications.[9,10]

One of the areas in which MOFs have received some reticence concerns their stability.[11] Indeed, some of the most well-known materials do not seem to be sufficiently stable to humidity, allowing their use in applications, with the exception of some bio-applications.[9,10] Furthermore, the synthesis route (hydrothermal, solvothermal, microwave) also has an influence on the final stability of the MOF.[12]

With these considerations in hand, one promising MOF is the UiO-66[13] solid which is built up from $[Zr_6O_4(OH)_4(CO_2)_{12}]$ clusters linked with 1,4-benzenedicarboxylic acid. It leads to an overall porous cubic architecture as illustrated in Figure 1. This structure is claimed to be thermally stable up to 813 K and to the dehydroxylation/rehydroxylation process. It contains a three-dimensional arrangement of micropores with each centric octahedral cage surrounded by eight corner tetrahedral cages (free diameters of approximately 11 and 8 Å for the two types of cages, respectively) and connected through narrow triangular windows (approximately 6 Å). In this structure, the triangular faces of the Zr_6-octahedron $Zr_6O_4(OH)_4$ are alternatively capped with four μ_3-O and four μ_3-OH groups.

[a] A. D. Wiersum, E. Soubeyrand-Lenoir, Dr. S. Bourrelly, Dr. C. Vagner, Dr. P. L. Llewellyn
Laboratoire Chimie Provence (UMR 6264)
Universités Aix-Marseille I, II et III - CNRS
Centre de Saint Jérôme, 13397 Marseille cedex 20 (France)
Fax: (+33) 491-637-111
E-mail: philip.llewellyn@univ-provence.fr

[b] Dr. Q. Yang, Dr. M. B. Yahia, Dr. G. Maurin
Institut Charles Gerhardt Montpellier (UMR 5253)
Université Montpellier II, CNRS, ENSCM
Place E. Bataillon, 34095 Montpellier cedex 05 (France)
Fax: (+33) 4 67 14 42 90
E-mail: guillaume.maurin@univ-montp2.fr

[c] Dr. B. Moulin, Dr. A. Vimont, Prof. M. Daturi, Dr. G. Clet
Laboratoire Catalyse et Spectrochimie
ENSICAEN, Université de Caen, CNRS
6 Bd Maréchal Juin, 14050 Caen (France)

[d] V. Guillerm, Dr. S. Miller, Dr. C. Serre
Institut Lavoisier (CNRS 8180)
CNRS - Université de Versailles St Quentin en Yvelines
45 avenue des Etats-Unis, 78035 Versailles (France)

Supporting information for this article is available on the WWW under http://dx.doi.org/10.1002/asia.201100201.

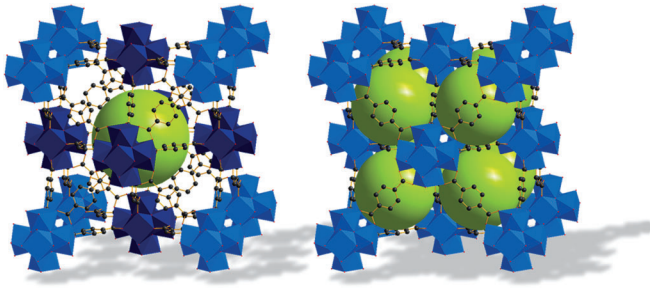

Figure 1. Schematic illustration of the UiO-66 structure: left octahedral cages, right tetrahedral cage. Zirconium polyhedra and carbon atoms are in blue and black, respectively. Hydrogen atoms are omitted for a better understanding.

One of the unusual structural features of this MOF phase is its supposed variation of the coordination number of the zirconium metal center between the hydroxylated (VIII) and dehydroxylated (VII) forms.[13] Such a local modification can influence the adsorption properties as is the case for the MIL-100(Cr, Fe) solid in which,[14,15] according to the activation conditions, a significant number of free metal sites are accessible and in the case of Fe^{3+}, a fraction of the metal centers can be reduced to Fe^{2+}.[15] The liberation of co-ordinatively unsaturated sites (cus) leads to significant variations in the enthalpies of adsorption for molecules such as CO and propylene.[15] In the case of UiO-66, the Zr^{VII} and Zr^{VIII} forms are expected to be structurally slightly different, and this may add a second parameter that could play a role on the gas adsorption properties.

The aim of the present work therefore was to explore the dehydroxylated form of UiO-66 from a structural and spectroscopic standpoint, prior to evaluating its stability towards humidity and further its adsorption properties with respect to industrially important gases, from an energy and environmental perspective, including methane, carbon monoxide, and carbon dioxide. Molecular simulations have been first used here to assist the structure determination from the X-ray powder diffraction data for the dehydroxylated form, which has not been addressed so far, and further to provide some insights into the host–guest interactions experimentally explored by spectroscopic (FTIR) and thermodynamic (adsorption/calorimetry) measurements. Beyond the scientific conclusions, this paper presents a strategy that can be taken for (1) determining if this class of material provides the necessary properties for industrial applications, including stability towards humidity and high temperature, and (2) evaluating their adsorption performance with respect to single gases, which is the first step to probe the potential of such materials for further storage/separation type applications.

Results and Discussion

Activation

The activation of the sample was carried out using thermogravimetric analysis (TGA) in high resolution mode, in which the heating rate of the sample is dynamically and continuously varied in response to changes in the sample's rate of decomposition.[16] This mode allows a better separation of successive events with respect to the standard linear heating rate mode. However, a standard linear heating mode coupled with evolved gas analysis was used to identify evolved species. In a separate series of experiments, the evolution of the various surface groups was followed by infrared spectroscopy.

The TGA curve obtained from the as-synthesized sample (Figure 2) shows several mass losses. The initial loss (14%) occurs at 303 K and the second (~2%) loss occurs below a temperature of 393 K. These first losses are most likely owing to free species from the external surface of the particles followed by the departure of physisorbed species from the pores. Two further small mass losses occur in the region from 473 to 673 K before a final large loss of almost 40% at higher temperatures. This final loss can be attributed to sample decomposition as confirmed by the evolved gas analysis and occurs in the region of 723 K with an onset at around 758 K. This latter temperature can thus be considered as the upper limit of sample stability, which is slightly lower than the temperature suggested previously (813 K).[13]

In order to confirm the evolution of organic species arising from sample degradation as well as to evaluate the species removed at each of the other steps, a second series of experiments were carried out with evolved gas analysis (Figure 3). These experiments show that the major species lost up to 673 K correspond to water with the characteristic ratio m/z peaks of 18 (17 and 16 are not shown in Figure 3 for simplification) being observed. This would therefore suggest that water is initially lost in the physisorbed state up to 423 K and that the weight loss at around 573 K corresponds to water, probably resulting from dehydroxylation. This latter point is confirmed by IR spectroscopy (see below). A small variation in the $m/z = 12$ and 28 peaks further hint at

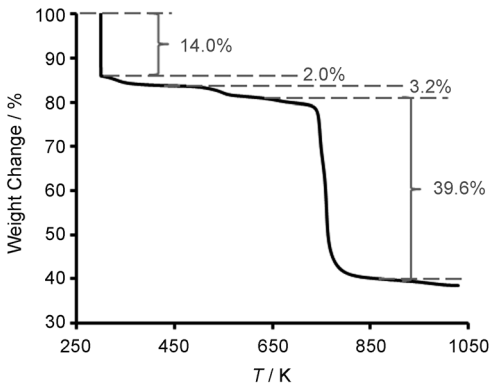

Figure 2. "Hi-Res" TGA curve in argon obtained with the as-synthesized UiO-66.

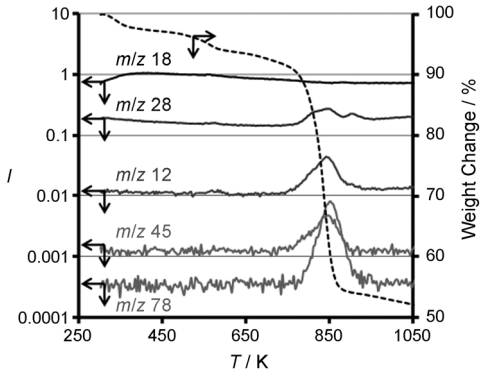

Figure 3. TG-MS curves recorded for UiO-66. Only the most significant fragments are reported.

the loss of organic species (*N*,*N*-dimethylformamide; (DMF)), which are more clearly observed by IR. As suggested above, the major weight loss arises from framework degradation with the observation of typical species owing to the phenyl ($m/z=78$) and carboxyl fragments ($m/z=45$).

Following the thermal treatment, using in situ IR spectroscopy further suggests that small amounts of impurities are also desorbed up to 573 K. Indeed, it seems that residual DMF, used in the synthesis protocol and characterized by the band at 1665 cm^{-1}, is still present in the sample. It is lost during the initial treatment under vacuum from room temperature up to 423 K (Figure 4). Traces of free terephthalic acid are also detected by the bands at 1732 and 1746 cm^{-1}, which disappear at around 523 K.

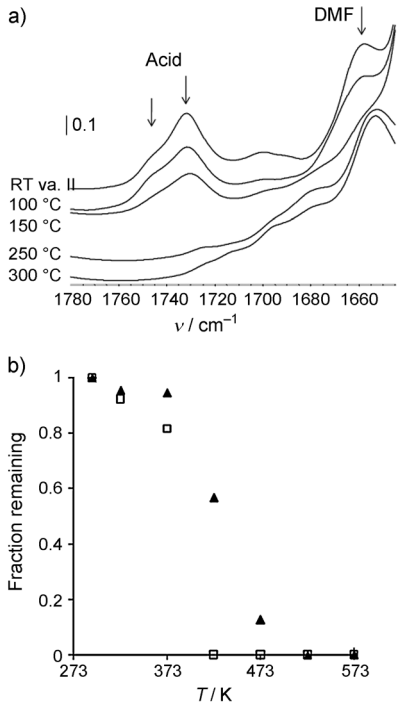

Figure 4. Influence of temperature of activation on the presence of organic impurities: a) FTIR spectra and b) fraction of impurities remaining after thermal treatment (□: DMF, ▲: free acid). The fractions of DMF and acid were calculated from the areas of the bands at ca. 1665 and 1740 cm^{-1} respectively and normalized to the values measured after evacuation at 298 K.

FTIR—Dehydroxylation Process

The thermal treatment of UiO-66 was studied by IR spectroscopy to follow the removal of the intra-framework OH group with temperature. Figure 5 shows the IR spectra of the solid in the hydroxyl region. Initially at 298 K, the solid exhibits a sharp band at 3674 cm^{-1} along with a smaller one at 3654 cm^{-1}, which is attributed to free hydroxyl groups. A broad band centered around 3400 cm^{-1} is assigned to perturbed hydroxyls, which significantly decreases upon evacuation at 298 K, thus revealing an additional shoulder at around 3440 cm^{-1}. Both the small band at 3654 cm^{-1} and the shoulder at 3440 cm^{-1} vanish above 373–423 K. These bands indicate some H-bonding with an adjacent basic center and are likely a result of the presence of impurities such as DMF or water.

The main hydroxyl band at 3674 cm^{-1} is similar to that observed for zirconia where it may be attributed to a doubly or triply bridged OH.[17,18] However, the well-defined structure of UiO-66 implies that the band at 3674 cm^{-1} arises from a triply-bridged OH. The presence of the same OH on zirconia is noteworthy and could be an indication to resolve its controversial assignment.

Calcination of the solid has a noticeable effect on the hydroxyl groups. The number of hydroxyl groups indeed strongly decreases upon thermal treatment (Figure 5) and

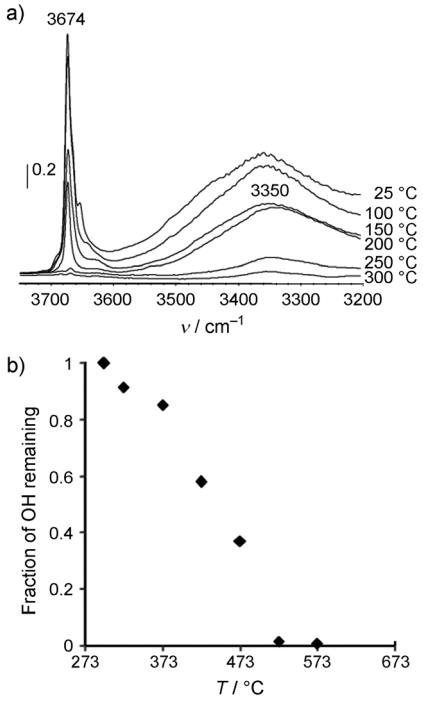

Figure 5. Influence of the temperature on the dehydroxylation: a) FTIR spectra of the hydroxyl groups and b) fraction of the unperturbed OH at 3674 cm^{-1} remaining after thermal treatment.

there are almost none above 523 K. Additional modifications of the spectrum occurred upon dehydroxylation in the regions of 1600–1300 and 750–500 cm^{-1}. They are coherent with the experimental and theoretical data of Valenzano and co-workers.[19]

After introduction of water vapor on the activated solid, the band at 3674 cm^{-1} was restored and the IR spectrum was finally similar to that obtained before dehydroxylation (not shown). This is consistent with the results published by Hafizovic Cavka[13] and Valenzano[19] and their respective co-workers, and implies that the introduction of water vapor induces the rehydroxylation of the solid with the consequent formation of hydroxyls similar to those present in the initial solid. Dehydroxylation and rehydroxylation are thus fully reversible, and this allows the possibility to carry out longer term cycling measurements in order to confirm the longer term stability of the sample as discussed in the following section.

Water Adsorption and Cycling Measurements

As mentioned above, the stability with respect to water and temperature can be an issue for MOFs. TGA confirms the stability of UiO-66 up to 758 K. Whilst it is possible to carry out hydrothermal testing on a large scale,[11] water adsorption–desorption cycling at a given temperature can give an idea of the stability of a given phase with respect to this vapor. In the present study, two series of experiments were carried out. First, two isotherms were obtained at 298 K with a regeneration step between runs at 353 K for 2 hours under inert gas flow. The two isotherms obtained coincide (Figure 6a). They are characterized by an initial low uptake to around 25% relative humidity (RH) at which point pore filling occurs in the RH range between 30% and 50% to a final plateau of around 0.37 $g\,g^{-1}$. The pore volume calculated from the water isotherms is 0.35 $cm^3{}_{Liq}\,g^{-1}$ which is close to that obtained by nitrogen porosimetry. The initial low uptake is similar to that observed for a number of carboxylate-based MOFs,[4,20,21] which is characteristic of a certain hydrophobicity of the activated UiO-66 material.

TGA results obtained with a fully activated and then rehydrated sample (Figure SI-1 in the Supporting Information) show two main steps up to 573 K corresponding to physisorbed species (lost up to 423 K) and to the structural dehydroxylation, corresponding to only 1.35% (423–593 K).

In a second series of experiments, the activated UiO-66 is subjected to five adsorption–desorption cycles (Figure 6b). A limited number of relative pressures are explored in order to allow for more cycles in a reasonable timescale (10 days). The second and following cycles are shifted with respect to the first one. This shift of around 3% suggests a partial rehydroxylation of the sample during the first run. However, the four consequent runs show the same uptakes for each relative pressure, thus suggesting that no degradation occurs under these conditions. In addition, the small shift of the isotherm to lower pressure during the first three cycles suggests a higher degree of hydrophilicity in agreement with a full hydroxylation of the zirconium oxide building unit after the third run, assuming that desorption at 353 K under inert atmosphere between each cycle leads to no dehydroxylation.

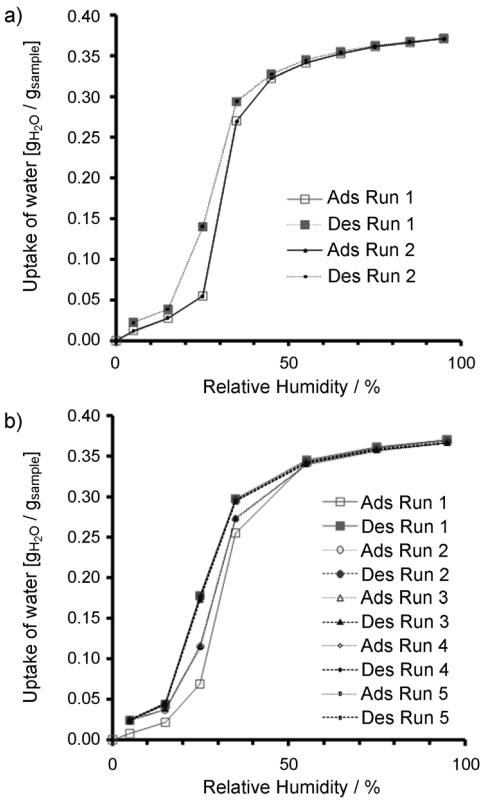

Figure 6. Water adsorption–desorption isotherms. a) Two cycles with regeneration at 353 K under an inert atmosphere and b) 5 cycles at 303 K with no thermal regeneration between cycles.

Computational Assisted Structure Determination

It was previously reported that the dehydroxylated UiO-66 structure results from the departure of two of the four μ_3-OH groups in each inner core together with the H atoms from the remaining two μ_3-OH groups. This rearrangement was supposed to lead to the formation of inner clusters, Zr_6O_6, with seven-coordinated Zr^{4+} metal centers. A high quality X-ray powder diffraction pattern has been obtained using a sample of UiO-66, introduced in a glass capillary, activated overnight at 523 K under high vacuum. An initial structural model for the dehydroxylated form has thus been built-up based on this observation and completed by structural information extracted from the X-ray analysis, combined with an energy minimization procedure based on classical interatomic potentials. Such an approach has been recently successfully employed to simulate the structures of various MOFs.[22,23] This model was used as a starting point for Rietveld refinement leading to the structure described in the Supporting Information, the space group symmetry and unit cell parameters being reported in Table 1.

Table 1. Comparison of the optimized crystallographic data for the hydroxylated and dehydroxylated UiO-66(Zr) with the experimental ones.

Crystallographic data	Hydroxylated		Dehydroxylated	
	Experimental	Calculated	Experimental	Calculated
a [Å]	20.7004	20.7937	14.1595	14.8598
b [Å]	20.7004	20.7937	14.1595	14.8598
c [Å]	20.7004	20.7937	34.1200	34.8904
Volume [Å^3]	8870.26	8990.80	5924.30	6672.07
space group	$Fm\bar{3}m$ (no. 225)	$F\bar{4}3m$ (no. 216)	$R\bar{3}m$ (no. 166)	$R\bar{3}m$ (no. 166)

Table 2. Comparison of the main crystallographic distances (Å) for the optimized hydroxylated and dehydroxylated UiO-66(Zr) with the experimental ones and the previous theoretical results from the literature.[19]

Neighbors[a]	Experimental	Calculated	Literature data
Hydroxylated			
O3	2.107	2.071	2.089
O2		2.258	2.286
O1	2.233	2.217	2.249
C1	3.255	3.232	3.267
C2	4.595	4.553	4.596
Zr	3.510	3.530	3.571
	4.964	4.992	5.050
Dehydroxylated			
O3	1.966	2.065	2.052
	2.324	2.163	2.060
			2.237
O1	1.987	2.184	2.193
	2.232	2.204	2.225
			2.227
			2.240
C1	3.031	3.189	3.203
	3.077	3.240	3.214
			3.243
			3.305
Zr	3.277	3.400	3.462
	3.400	3.705	3.736
	4.722	5.029	5.093

[a] The labels of the neighbors can be found in Figure SI–2 in the Supporting Information, and the distances were measured form one Zr atom to its various types of neighbors.

In parallel, the initial structural model has also been fully optimized in its primitive cell by using periodic density functional theory calculations (see the detail given in the Supporting Information). The optimized unit cell parameters are reported in Table 1 and these values compare well with the experimental data. The cif file of this resolved structure is provided in the Supporting Information.

The overall framework structure of the dehydroxylated form is indeed very similar to the hydroxylated version and keeps the same organization of the two types of cages, that is, each centric octahedral cage is surrounded by eight corner tetrahedral cages through narrow windows. In addition, although two of the four μ_3-OH groups and the H atoms from the remaining two μ_3-OH groups are removed from the framework during the dehydroxylation, the bond distances between the different atoms in the inorganic nodes remain almost identical in these two forms. As a typical illustration, in the simulated dehydroxylated form, the average Zr–O carboxylate and Zr–μ_3O bond distances are 2.194 and 2.114 Å, respectively, which compare well with those present in the hydroxylated form, that is, 2.217 and 2.071 Å (see Table 2). From a fair agreement with both our experimental crystallographic data and those theoretically reported elsewhere,[19] one can be confident with the proposed model. Finally, we confirm here that the coordination number of zirconium goes from VIII to VII upon full dehydroxylation. It should be noted that the hexagonal structural model of the dehydroxylated UiO-66 assumes that all the Zr_6-octahedron $Zr_6O_4(OH)_4$ are orientated in the same direction. This model only slightly deviates from those recently proposed by Valenzano and co-workers,[19] with a trigonal $R\bar{3}m$ (no. 148) space group.

Adsorption of CO and CO_2 followed by FTIR

The above results (TGA, IR, XRPD) suggest that UiO-66 is stable with respect to water, with a gradual dehydroxylation up to around 523 K. This behavior allows a study of the UiO-66 at various stages of dehydroxylation using various probe gases. The interaction of the solid with CO and CO_2 was followed by FTIR to study the molecular interactions. Furthermore, adsorption microcalorimetry was used to characterize the energetics during the adsorption of both CO and CO_2 as well as CH_4.

Carbon monoxide is an IR probe, which can be used to follow the acidity of the sample. The adsorption of CO was carried out at room temperature before and after dehydroxylation. However, in both cases, hardly any adsorption was observed, indicating very weak acidity. The experiment was thus repeated at low temperature to probe the weakest sites. Figure 7 presents the results of CO adsorption recorded at low temperature (77 K) after dehydroxylation of the sample at 523 K. Upon CO introduction by successive aliquots (indicated by the arrows), a strong band is present at 2155 cm^{-1}. In parallel, the signature of the hydroxyl group

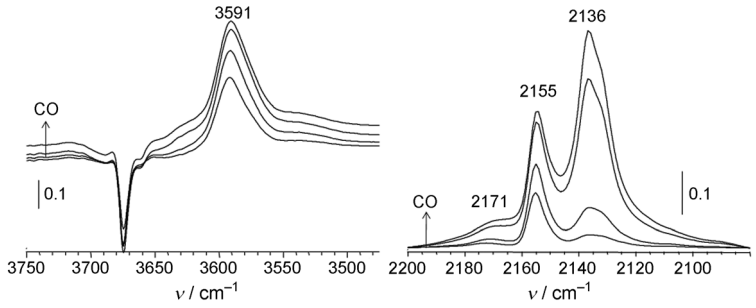

Figure 7. FTIR spectra after adsorption of increasing amounts of CO at 77 K after dehydroxylation. The spectra were obtained after subtraction of the solid before adsorption.

at 3674 cm^{-1} is perturbed, thus leading to a new band at 3591 cm^{-1}. This shift ($\Delta\nu(OH) = 83\ cm^{-1}$) is consistent with the position of the CO band at 2155 cm^{-1} and it is thus attributed to CO hydrogen bonded with Brønsted sites of a weak acid strength. This shift is similar to that obtained when CO interacts with the hydroxyls of zirconia (band at 3665–3675 cm^{-1}).[24]

A weak band was also observed at 2172 cm^{-1}. This feature cannot be related to another shift of the hydroxyls and it is thus attributed to a small amount of CO coordinated to Zr Lewis acid sites. At higher CO loading, a band at approximately 2136 cm^{-1} (with a shoulder at 2132 cm^{-1}) appeared which is assigned to physisorbed CO.

The absence of strong sites, regardless of the hydroxylation state, was confirmed by the adsorption of CO_2 (Figure 8). These results show that the dehydroxylation does not modify the interactions of the solid with CO_2 at low pressure. On both the solids evacuated at 323 K or at 523 K, only one band owing to physisorbed CO_2 has been observed at 2339 cm^{-1}, the variation of which as a function of pressure is similar on both the hydroxylated and dehydroxylated forms (Figure 8c). This band equally disappears after evacuation at ambient temperature, confirming the weak interaction between CO_2 and the surface. As a comparison, Morterra and co-workers have studied the adsorption of CO_2 on

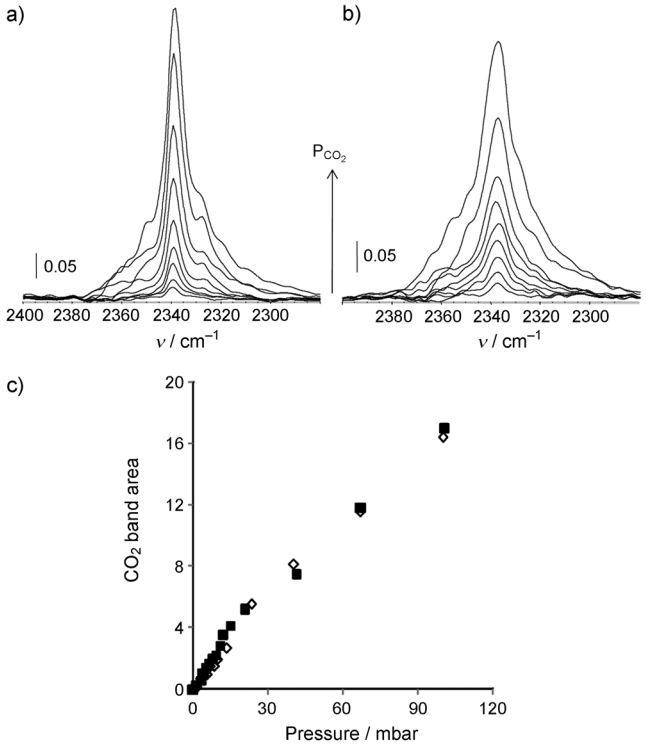

Figure 8. Adsorption of 1–100 mbar CO_2 followed by FTIR. Spectra a) of the hydroxylated form and b) of the dehydroxylated form; c) Quantification of adsorbed CO_2 (◇: hydroxylated form, ■: dehydroxylated form). The spectra were obtained after subtraction of the spectrum of the solid before adsorption and of CO_2 in the gas phase. For the quantification, the band areas were normalized with the structure bands to account for the variations in mass for each sample analyzed.

monoclinic zirconia.[24,25] In this case, activation at low temperature induced the appearance of a CO_2 band at 2355 cm^{-1} while activation above 600 K induces the existence of a band at 2365 cm^{-1}, which both are attributed to CO_2 coordinated on the Lewis acid sites of zirconia. The absence of characteristic CO_2 bands at wavenumbers higher than 2340 cm^{-1} in the spectra of UiO-66 confirms that there are no coordinated species.

The interactions between CO or CO_2 and UiO-66 sites are clearly not comparable to the ones measured on zirconia as these probes do not lead to the formation of coordinated species whatever the hydroxylation state. The absence of any strong interaction between CO or CO_2 and the UiO-66 surface for any hydroxylation state was confirmed by calorimetry experiments and molecular simulations (see below).

Adsorption Calorimetry of CO_2, CH_4, and CO at 303 K

The exploration of the stability to water of UiO-66 and the TGA and FTIR experiments permit an estimation of the degree of hydroxylation after various thermal treatments of the initially fully hydrated material. The effect of various degrees of hydroxylation on the adsorption of various topical probe gases at 303 K has been evaluated here.

Carbon dioxide is a useful probe for calorimetry as, with its quadrupole moment of $-14.98 \times 10^{-40}\ C\,m^2$, it is able to probe variations in the chemistry of most surfaces. Figure 9 shows the isotherms (Figure 9a) and differential enthalpies of adsorption of CO_2 (Figure 9b) obtained at 303 K on the UiO-66 outgassed to various temperatures. The various outgassing temperatures lead to various hydroxylated states of the sample.

The different CO_2 isotherms are all of Langmuir type (Figure 9a), with only small variations in uptake depending on the outgassing temperature. This is confirmed by the GCMC calculations. Indeed, the simulated isotherms obtained for both the dehydroxylated and hydroxylated forms are in good overall agreement with the experimental data for both the sample activated at 353 K and at 523 K (Figure 9b), which is thought to be hydroxylated and fully dehydroxylated, respectively, as discussed above. However, a small but significant increase in the uptake is observed on outgassing from 303 K to 353 K, and this which can be related to the loss of physisorbed water leading either to a slightly larger available pore volume and/or to an easier accessibility for CO_2 to the structural hydroxyl groups. When further increasing the temperature from 150 °C to 300 °C, the uptake at 10 bar slightly decreases which was unexpected as the total accessible pore volume of the sample should increase slightly upon dehydroxylation.

To shed some light on this "surprising" decrease in CO_2 capacity upon activation at temperatures higher than 353 K, direct measurements of the differential enthalpies of adsorption using microcalorimety were made (Figure 9b). Both profiles and values at low coverage have been considered to characterize the samples. Two series of curves can be seen. First, for the samples outgassed below 423 K, the initial en-

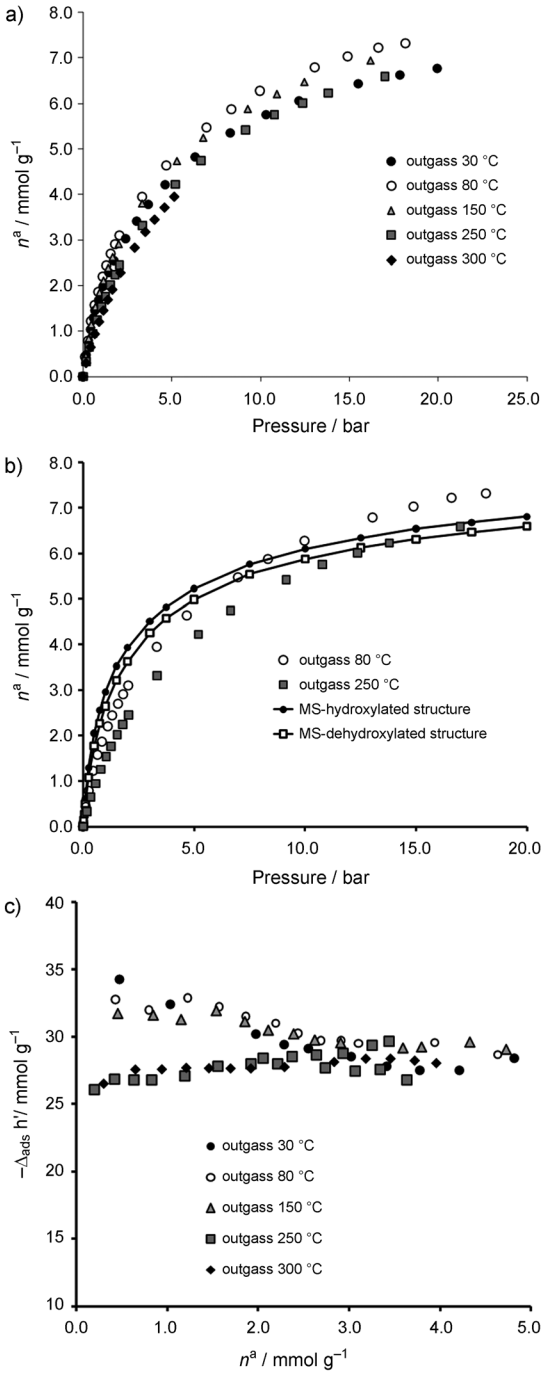

Figure 9. CO_2 adsorption at 303 K on UiO-66. a) Isotherms after outgassing to various temperatures. b) Comparison between experimental and molecular simulated (MS) isotherms on the hydroxylated and dehydroxylated froms of UiO-66. c) Differential enthalpies of adsorption measured by microcalorimetry.

thalpies are quite similar in the range of −32 to −35 kJ mol^{-1} and one observes an initial decrease in the calorimetric curve prior to a plateau region above 3 mmol g^{-1} with an enthalpy value centered around −26.5 ± 0.5 kJ mol^{-1}, in good agreement with the simulated enthalpy at low coverage (for ca. 1 mmol g^{-1}) for the hydroxylated structure value of −26.1 kJ mol^{-1}. Such an enthalpy profile is usually characteristic of a heterogeneous energetic surface experienced by CO_2. Secondly, for the samples outgassed to above 473 K, a region where the FTIR measurements suggest that dehydroxylation is complete, a different calorimetric curve is observed with only a slightly increasing profile with an enthalpy value centered around −26.0 kJ mol^{-1} which fits well with the simulated enthalpy for the dehydroxylated structure (−25.3 ± 0.5 kJ mol^{-1}). One further observes that both experimental and simulated values are very similar to the ones obtained on the plateau observed for the hydroxylated structure, consistent with a similar strength of CO_2–UiO-66 interactions in both forms as shown by the infrared measurements. This shape of calorimetric curve is indicative of a homogeneous energetic surface in which increasing gas–gas lateral interactions are superposed on a constant interaction of the probe with the solid as previously pointed out for CO_2 adsorbed on the dealuminated Y faujasite.[26] Interestingly, the curves obtained after outgassing either to 523 K or 573 K almost overlap, indicating a similar energetic state after treating to higher temperatures.

However, there is a strong discrepancy between the initial enthalpies of adsorption for the sample activated at low temperature (303–423 K). One can rule out the effect of traces of basic DMF moieties or free terephthalic moieties as the sample was initially activated at high temperature prior to rehydration and CO_2 sorption experiments. Despite the presence of hydroxyl groups, molecular modelling does not indicate any significant difference in host–guest interactions whilst a 6–9 kJ mol^{-1} difference in energy of the interaction is measured experimentally. As shown previously with the copper based MOF HKUST-1, the presence of free water at low loading (4 wt %) seems to enhance the adsorption of CO_2.[27] Here, it is likely that any remaining water molecules leads to additional interactions within the whole system, that could be at the origin of the higher enthalpy of adsorption observed at low loading. In addition, IR and TGA analysis have shown that free water and hydroxyl groups decrease in parallel. This is consistent with previous IR dehydration experiments performed on MIL-100-Cr where the departure of free and bound water were not fully separated.[14] It was shown indeed that in addition to a very large amount of weakly bound physisorbed water, one free water molecule has a strong interaction with each water molecule coordinated to the Lewis chromium acid sites. Further, owing to the distribution of Lewis acid strengths, the departure of some weakly bound coordinated water molecules probably occurs prior to the full departure of all free water molecules. Indeed, one can imagine for UiO-66 a similar phenomenon as IR and TGA do not clearly distinguish the departure of water molecules and hydroxyl groups. One therefore expects that a few residual free water molecules are left, upon activation below 423 K, and have a strong interaction with remaining hydroxyl groups which thus provide stronger adsorption sites for CO_2.

A further step consists in probing the geometric arrangements of the different adsorbates in the hydroxylated form

CHEMISTRY
AN ASIAN JOURNAL

at low pressure. All adsorbates are preferentially located in the tetrahedral cages. The average distance between the protons of the −OH group and the oxygen atoms of both CO_2 and CO is about 2.36 Å and 2.77 Å, respectively, as illustrated in Figure 10, which is characteristic of a rather weak host–guest interaction, consistent with FTIR measurements.

It is worth noting that the enthalpies obtained here are well below those observed with zirconium oxides, the initial interactions of which are around $-130\,kJ\,mol^{-1}$,[28,29] while the value at the plateau remains significantly lower than for other MOF materials, including HKUST-1 ($-36\,kJ\,mol^{-1}$[30]) and MIL-53Cr ($-35\,kJ\,mol^{-1}$[5]). In addition, the so-obtained enthalpies observed for these MOFs are much lower than those of many zeolites including NaY ($-49\,kJ\,mol^{-1}$[31]), thus suggesting that the MOFs can be regenerated under milder conditions than their zeolitic counterparts, even for very polar MOFs with accessible cus. Indeed, both the isotherm and enthalpy on the desorption curves (not shown) are completely reversible.

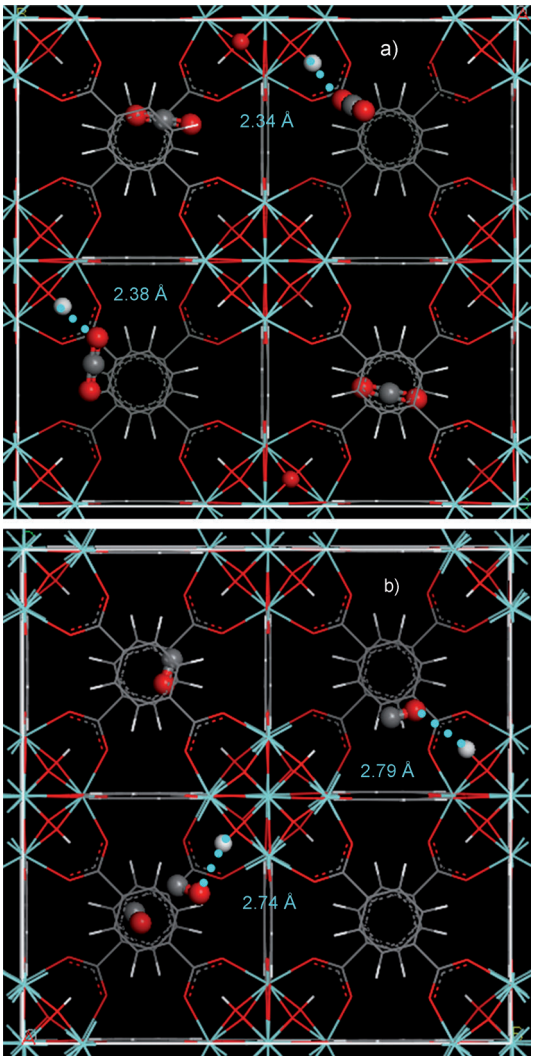

Figure 10. Typical illustration of the interactions between the hydroxylated UiO-66(Zr) structure with a) CO_2 at 0.1 bar and b) CO at 2.5 bar. The characteristic distances are reported in Å.

Methane is a useful probe molecule in calorimetry measurements as it can be considered quite neutral with no permanent moment. It is quite insensitive to variation of the surface chemistry but can highlight changes if the topology varies significantly. In the present case, both the isotherms and calorimetric curves obtained for methane adsorption for both fully hydroxylated and dehydroxylated samples (Figure 11) are quite similar, which confirms that there is no major change in the structure of the material when one goes from dehydroxylated to hydroxylated forms. The simulated adsorption enthalpy at low coverage is −18.80 and $-18.90\,kJ\,mol^{-1}$ in the dehydroxylated and hydroxylated forms, respectively (Figure 12), consistent with the experimental value of around $-18.5\,kJ\,mol^{-1}$, extrapolated from Figure 11b, thereby confirming very similar strength of interactions with the UiO-66 surface. These values are again in the same region as those observed for many MOFs whether they be small pore (ScBDC: $-17\,kJ\,mol^{-1}$[32]), medium pore (MIL-53Cr: $-17\,kJ\,mol^{-1}$[5]) or large pore (MIL-100/MIL-101: $-18\,kJ\,mol^{-1}$[33]).

In the case of carbon monoxide (Figures 11 and 12), the same trend, as for CH_4, has been observed both for the simulated and experimental adsorption isotherms regardless of the hydroxylation state. The resulting adsorption enthal-

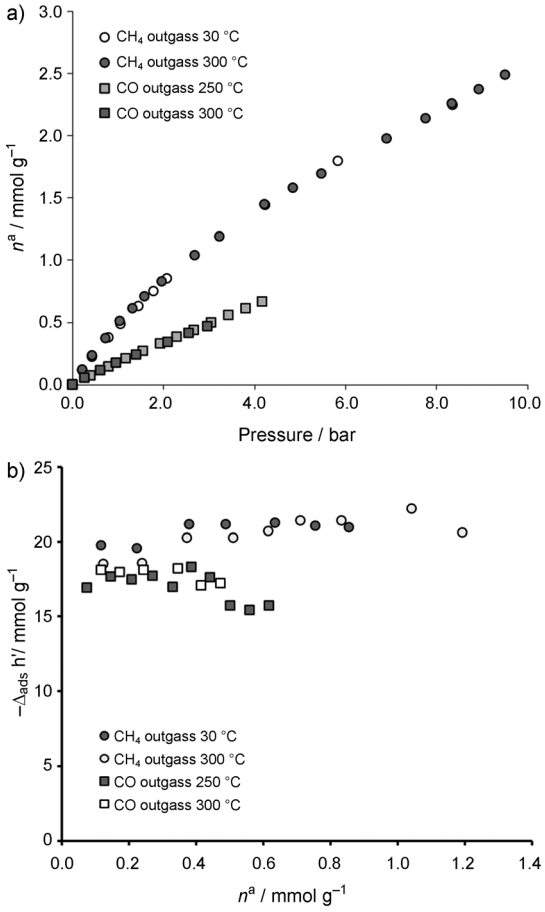

Figure 11. Adsorption of CO and CH_4 at 303 K on UiO-66. a) Adsorption isotherms and b) differential enthalpies of adsorption.

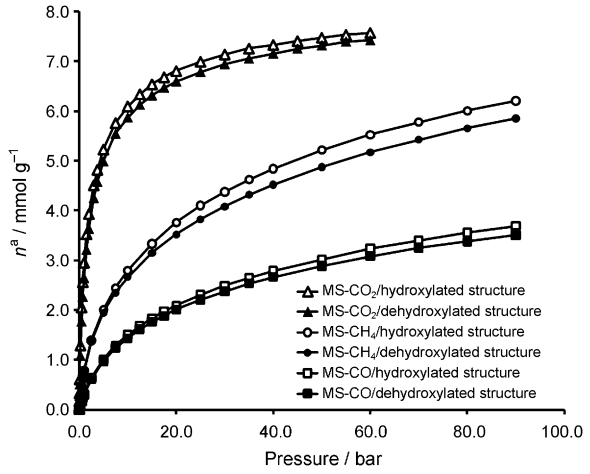

Figure 12. Molecular Simulation (MS) data of high pressure isotherms of CH_4, CO, CO_2 at 303 K on the hydroxylated and dehydroxylated forms of UiO-66.

pies at low coverage are almost the same for both forms, centered around $-16.0\,kJ\,mol^{-1}$ and $-16.6\,kJ\,mol^{-1}$ from calorimetry and simulations, respectively, corresponding to an energetic region similar to that found for crystalline zirconia $-18\,kJ\,mol^{-1}$.[34] When comparing with other MOFs, the value obtained here compares well with MIL-53Cr ($-17\,kJ\,mol^{-1}$[6]), which also contains hydroxyl groups. ScBDC, which has no specific adsorption sites, leads to a lower initial enthalpy of $-13\,kJ\,mol^{-1}$.[32] However, a MOF with free metal cus, such as reduced MIL-100(Fe), gives initial adsorption enthalpies of around $-51\,kJ\,mol^{-1}$.[15] This behavior therefore confirms the results from IR that the CO interacts with quite weak adsorption sites.

A comparison of the CO_2 adsorption capacity of the UiO-66 with other known porous materials is given in Figure 13. Here, the amount of gas adsorbed is given in volume of CO_2 per volume of solid. The crystallographic densities for MOFs and zeolites have been used to make this comparison as it is difficult to sufficiently activate these highly porous samples in a standard helium pycnometer. It should be also considered that in a real application, packing densities will be used to give a final "real" comparison. Nevertheless, this gives a convenient comparison of the UiO-66 with a reference zeolite, NaY, and other well documented high CO_2 capacity MOFs such as MIL-100, MIL-101,[33] and MOF177.[35] One can note a more rapid uptake of the NaY at low pressure and a comparable final uptake of the NaY with the UiO-66 above a pressure of around 15 bar. This is directly related to the higher adsorption enthalpy and thus to the relative ease (or not) of sample regeneration. Interestingly, in the low and medium pressure range up to 15 bar, a comparable uptake is observed between the UiO-66, MIL-100, and MIL-101 samples. Nevertheless, a closer inspection shows that at very low pressures (below 1 bar), the MIL samples show an enhanced uptake owing to the presence of cus. While in the medium pressure range, a slightly higher uptake is observed for UiO-66, which can be related to the

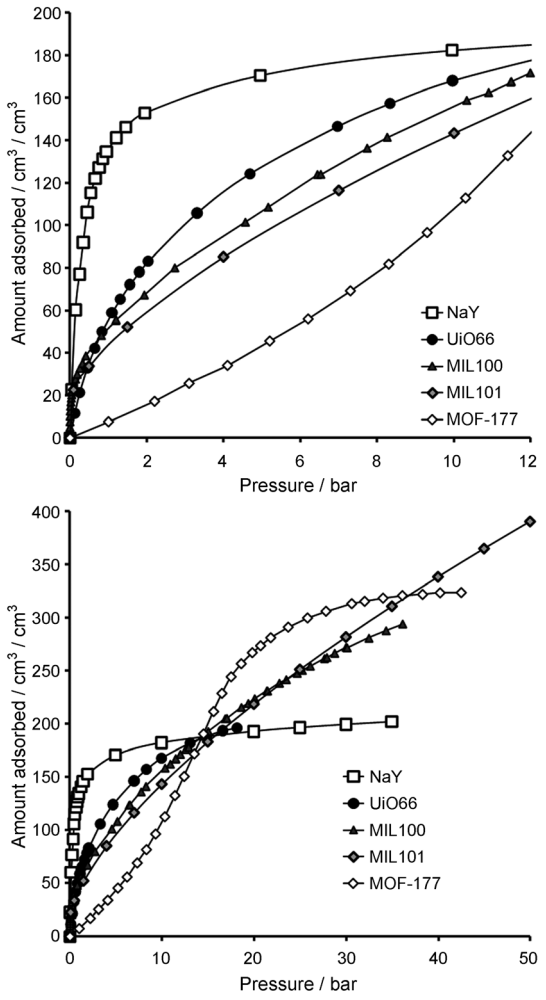

Figure 13. Comparison, in volume per volume, of the adsorption of CO_2 at 303 K of UiO-66 with other MOFs (MIL100, MIL101, MOF177) and a reference zeolite (NaY).

smaller pore size. In this low to medium pressure range, MOF-177 shows a more limited uptake, although at higher pressures, MOF-177 exhibits a very large uptake owing to a higher accessible pore volume. Above 40 bar, MIL-101 shows finally the highest CO_2 adsorption capacity. The comparison with NaY is the most relevant in terms of volumetric uptake with the additional possibility that the UiO-66 is more easily regenerated. Further work with respect to the effect of water on CO_2 adsorption will be of interest, as it is known that water has a detrimental effect on CO_2 uptake with NaY, whilst it is suggested that small quantities of water may help the uptake[27] and/or separation properties[36] of CO_2 on other MOFs.

Conclusions

The very high thermal stability of UiO-66 has been assessed as well as its stability to adsorption/desorption of water. The crystal structure of the dehydroxylated form has been deter-

mined and confirms the decrease in coordination number of zirconium upon dehydroxylation. Its evaluation with respect to the adsorption of topical gases (CO_2, CO, CH_4) suggests that the sample pretreatment has only a negligible effect on the adsorption capacities and as such, makes this sample of interest for further studies. Indeed, this sample has very limited acidic properties with only moderate interactions with polar gases such as carbon oxides, which, in addition to its valuable adsorption volumetric capacities and which are comparable to or better than the reference zeolite NaY (Figure 13) at intermediate pressure, makes UiO-66 of interest for CO_2 capture. The advantage of UiO-66 with respect to the zeolite resides in its larger dynamic capacity (that is, between 1 bar and 10 bar for instance) and its easier regeneration. Future studies will investigate these points and the adsorption properties of gas mixtures.

Experimental Section

Synthesis

UiO-66 was prepared as described previously[37] from a large scale mixture of zirconium tetrachloride $ZrCl_4$, terephthalic acid $HO_2CC_6H_4CO_2H$, hydrochloric acid (37%), and dimethylformamide in the 25 mmol:50 mmol:50 mmol:150 mL ratio. The slurry was then introduced into a 750 mL Teflon liner and then into a metallic PAAR bomb. The system was then heated overnight (16 h) at 493 K. The resulting white product was filtered off, washed with DMF to remove the excess of unreacted terephthalic acid, then washed with acetone, and finally dried at room temperature. Except for the study of the activation step (TGA and FTIR) where an as-synthesized solid was used, the sample was calcined at 523 K under vacuum (5 mbar) to remove the DMF from the framework before use.

Characterization

A structural model for UiO-66 dehydroxylated was determined by using a combination of X-ray powder diffraction data (XRPD), collected on a Bruker D8 diffractometer, and energy minimization procedure, based on Universal forcefield as implemented in the Materials Studio program suite. More details are provided in the Supporting Information. TGA experiments were carried out using a Q500 (TA Instruments) in both "Hi-Res" and linear heating mode. Evolved species were analyzed with a mass spectrometer Thermostar SM GSD 301 QMS 200. IR spectra were recorded with Nicolet Nexus or 6700 FT-IR spectrometers either on self-supported pellets or supported on a Si wafer. Water adsorption was carried out by using a gravimetric device (Q5000SA TA Instruments), which combines a high-sensitivity thermobalance and a humidity control chamber. The microcalorimetry experiments were carried out at 303 K by means of a homemade manometric dosing apparatus linked to the sample cell housed in a Tian-Calvet type microcalorimetrer.[38] An error of ± 1 kJ mol^{-1} can be considered for these experiments. The gases used for the adsorption were obtained from Air Liquide and were of 99.998% purity or better.

Molecular Simulations

The initial periodic structures of UiO-66 in the dehydroxylated and hydroxylated forms were built from their structural information extracted from the X-ray analysis. These models were then further fully optimized by density functional theory (DFT) calculations. Subsequently, grand canonical Monte Carlo (GCMC) simulations were performed to elucidate the adsorption behaviors of CO_2, CO, and CH_4 gases in these two optimized structures. For current studies, the intermolecular interactions between adsorbate as well as adsorbate–adsorbent were represented by a combination of short-range van der Waals (Lennard Jones) and long-range Coulombic interactions. The former were estimated by using a cut-off radius of 14 Å, while the latter were calculated using the Ewald summation. In our simulations, the systems were allowed to equilibrate for 1.5×10^7 MC cycles, followed by the production runs of another 1.5×10^7 MC steps. The atomic positions of the solids were frozen during the simulation. Further information about the force fields, partial charges of the framework atoms in MOFs, as well as the simulation protocol can be found in the Supporting Information. All these GCMC calculations were conducted using our own developed code ?CADSS? (Complex Adsorption and Diffusion Simulation Suite).

DFT Structural Optimization

The experimentally constructed periodic model was optimized by density functional theory (DFT) calculation, in which both atomic positions and lattice parameters were fully relaxed using a standard conjugate gradient. These calculations were performed using the Vienna ab initio simulation package (VASP) based on the project-augmented-wave method of Blochl and the plane-wave basis set with an energy cut-off of 600 eV. A k-point mesh of 2x2x2 was considered for sampling the Brillouin while the PBEsol exchange correlation functional was employed.

Acknowledgements

The research leading to these results has received funding from the European Community's Seventh Framework Programme (FP7/2007-2013) under grant agreement no. 228862. The authors would like to thank Dr. Yaroslav Filinchuk at the SNBL-ESRF for X-ray powder diffraction measurements. ADW, ELS, and PLL would like to thank Dominique Vincent and Christophe Giovannangeli for technical assistance.

[1] G. Férey, *Chem. Soc. Rev.* **2008**, *37*, 191.
[2] J. L. C. Rowsell, O. M. Yaghi, *Microporous Mesoporous Mater.* **2004**, *73*, 3.
[3] S. Horike, S. Shimomura, S. Kitagawa, *Nat. Chem.* **2009**, *1*, 695.
[4] M. Latroche, S. Surblé, C. Serre, C. Mellot-Draznieks, P. L. Llewellyn, J.-H. Lee, J.-S. Chang, S. H. Jhun, G. Férey, *Angew. Chem.* **2006**, *118*, 8407; *Angew. Chem. Int. Ed.* **2006**, *45*, 8227.
[5] S. Bourrelly, P. L. Llewellyn, C. Serre, F. Millange, T. Loiseau, G. Férey, *J. Am. Chem. Soc.* **2005**, *127*, 13519.
[6] S. Bourrelly, B. Moulin, A. Rivera, G. Maurin, S. Devautour-Vinot, C. Serre, T. Devic, P. Horcajada, A. Vimont, G. Clet, M. Daturi, J. C. Lavalley, S. Loera-Serna, R. Denoyel, P. L. Llewellyn, G. Férey, *J. Am. Chem. Soc.* **2010**, *132*, 9488.
[7] L. Alaerts, C. E. A. Kirshhock, M. Maes, M. A. van der Veen, V. Finsy, A. Depla, J. A. Martens, G. V. Baron, P. A. Jacobs, J. F. M. Denayer, D. E. De Vos, *Angew. Chem.* **2007**, *119*, 4371–4375; *Angew. Chem. Int. Ed.* **2007**, *46*, 4293–4297.
[8] I. Beurroies, M. Boulhout, P. L. Llewellyn, B. Kuchta, G. Férey, C. Serre, and R. Denoyel, *Angew. Chem.* **2010**, *122*, 7688–7691; *Angew. Chem. Int. Ed.* **2010**, *49*, 7526–7529.
[9] P. Horcajada, T. Chalati, C. Serre, B. Gillet, C. Sebrie, T. Baati, J. F. Eubank, E. Heurtaux, P. Clayette, C. Kreuz, J-S. Chang, Y. K. Hwang, V. Marsaud, P-N. Bories, L. Cynober, S. Gil, G. Férey, P. Couvreur, R. Gref, *Nat. Mater.* **2010**, *9*, 172.
[10] A. C. McKinlay, R. E. Morris, P. Horcajada, G. Férey, R. Gref, P. Couvreur, and C. Serre, *Angew. Chem.* **2010**, *122*, 6400; *Angew. Chem. Int. Ed.* **2010**, *49*, 6260.
[11] J. J. Low, A. I. Benin, P. Jakubczak, J. F. Abrahamian, S. A. Faheem, R. R. Willis, *J. Am. Chem. Soc.* **2009**, *131*, 15834.
[12] P. Chowdhury, C. Bikkina, D. Meister, F. Dreisbach, S. Gumma, *Microporous Mesoporous Mater.* **2009**, *117*, 406.
[13] J. H. Cavka, S. Jakobsen, U. Olsbye, N. Guillou, C. Lamberti, S. Bordiga, K. P. Lillerud, *J. Am. Chem. Soc.* **2008**, *130*, 13850.
[14] A. Vimont, J.-M. Goupil, J.-C. Lavalley, M. Daturi, S. Surblé, C. Serre, F. Millange, G. Férey, N. Audebrand, *J. Am. Chem. Soc.* **2006**, *128*, 3218.

[15] J. Y. Yoon, Y.-K. Seo, Y. K. Hwang, J.-S. Chang, H. Leclerc, S. Wuttke, P. Bazin, A. Vimont, M. Daturi, E. Bloch, P. L. Llewellyn, C. Serre, P. Horcajada, J.-M. Grenéche, A. E. Rodrigues, G. Férey, *Angew. Chem.* **2010**, *122*, 6085; *Angew. Chem. Int. Ed.* **2010**, *49*, 5949.
[16] P. Llewellyn, F. Rouquerol, J. Rouquerol, Ch. 6 in *Sample Controlled Thermal Analysis: Origin, Goals, Multiple Forms, Applications, and Future* (Eds.: O. Toft Sorensen, J. Rouquerol), Kluwer Acad. Publishers, Dordrecht, **2003**, 135.
[17] C. Morterra, G. Cerrato, L. Ferroni, L. Montanaro, *Mater. Chem. Phys.* **1994**, *37*, 243.
[18] M. Daturi, E. Finocchio, C. Binet, J. C. Lavalley, F. Fally, V. Perrichon, *J. Phys. Chem. B* **1999**, *103*, 4884.
[19] L. Valenzano, B. Civalleri, S. Chavan, S. Bordiga, M. H. Nilsen, S. Jakobsen, K. P. Lillerud and C. Lamberti, *Chem. Mater.* **2011**, *23*, 1700.
[20] P. Küsgens, M. Rose, I. Senkovska, H. Frode, A. Henschel, S. Siegle, S. Kaskel, *Microporous Mesoporous Mater.* **2009**, *120*, 325–330.
[21] Z. Liang, M. Marshall, A. L. Chaffee, *Microporous Mesoporous Mater.* **2010**, *132*, 305.
[22] T. Devic, P. Horcajada, C. Serre, F. Salles, G. Maurin, B. Moulin, D. Heurtaux, G. Clet, A. Vimont, J. M. Grenèche, B. Le Ouay, F. Moreau, E. Magnier, Y. Filinchuk, J. Marrot, J. C. Lavalley, M. Daturi, G. Férey, *J. Am. Chem. Soc.* **2010**, *132*, 1127.
[23] F. Salles, G. Maurin, C. Serre, P. L. Llewellyn, C. Knöfel, H. J. Choi, Y. Filinchuk, L. Oliviero, A. Vimont, J. Long, G. Férey, *J. Am. Chem. Soc.* **2010**, *132*, 13782.
[24] C. Morterra, G. Cerrato and S. Di Ciero, *Appl. Surf. Sci.* **1998**, *126*, 107.
[25] C. Morterra and L. Orio, *Mater. Chem. Phys.* **1990**, *24*, 247.
[26] G. Maurin, P. L. Llewellyn, R. G. Bell, *J. Phys. Chem. B* **2005**, *109*, 16084.
[27] J. Liu, Y. Wang, A. I. Benin, P. Jakubczak, R. R. Willis, V. M. D. Le, *Langmuir* **2010**, *26*, 14301.
[28] A. Auroux, A. Gervasini, *J. Phys. Chem.* **1990**, *94*, 6371.
[29] B. Bachiller-Baeza, I. Rodriguez-Ramos, A. Guerrero-Ruiz, *Langmuir* **1998**, *14*, 3556.
[30] Q. M. Wang, D. Shen, M. Bülow, M. L. Lau, S. Deng, F. R. Fitch, N. O. Lemcoff, J. Semanscin, *Microporous Mesoporous Mater.* **2002**, *55*, 217.
[31] J. A. Dunne, M. Rao, S. Sircar, R. J. Gorte, A. L. Myers, *Langmuir* **1996**, *12*, 5896.
[32] S. R. Miller, P. A. Wright, T. Devic, C. Serre, G. Férey, P. L. Llewellyn, R. Denoyel, L. Gaberova, Y. Filinchuk, *Langmuir* **2009**, *25*, 3618.
[33] P. L. Llewellyn, S. Bourrelly, C. Serre, A. Vimont, M. Daturi, L. Hamon, G. De Weireld, J. S. Chang, D. Y. Hong, Y. K. Hwang, S. H. Jhung, G. Férey, *Langmuir* **2008**, *24*, 7245.
[34] M. R. Alvarez, M. J. Torralvo, Y. Grillet, F. Rouquerol, J. Rouquerol, *Stud. Surf. Sci. Catal.* **1994**, *87*, 293.
[35] A. R. Millward, O. M. Yaghi, *J. Am. Chem. Soc.* **2005**, *127*, 17998.
[36] P. L. Llewellyn, S. Bourrelly, C. Serre, Y. Filinchuk, G. Férey, *Angew. Chem.* **2006**, *118*, 7915; *Angew. Chem. Int. Ed.* **2006**, *45*, 7751.
[37] P. S. Bárcia, D. Guimarães, P. A. P. Mendes, J. A. C. Silva, V. Guillerm, H. Chevreau, C. Serre, A. E. Rodrigues, *Microporous Mesoporous Mater.* **2011**, *139*, 67.
[38] P. L. Llewellyn, G. Maurin, *Comptes Rendus Chimie.* **2005**, *8 (3–4)*, 283.

Received: February 25, 2011
Published online: September 28, 2011

